Characterization of Ligand Effects on Water Activation in Triarylphosphine-Stabilized Pt Nanoparticle Catalysts by X-ray Absorption Spectroscopy

ARTICLE *in* THE JOURNAL OF PHYSICAL CHEMISTRY C · MARCH 2008

Impact Factor: 4.77 · DOI: 10.1021/jp709588c

7 AUTHORS, INCLUDING:

Olga A. Baturina
United States Naval Research Laboratory
63 PUBLICATIONS **614** CITATIONS
SEE PROFILE

Yannick Garsany
United States Naval Research Laboratory
35 PUBLICATIONS **538** CITATIONS
SEE PROFILE

Karen E. Swider-Lyons
United States Naval Research Laboratory
105 PUBLICATIONS **1,510** CITATIONS
SEE PROFILE

Characterization of Ligand Effects on Water Activation in Triarylphosphine-Stabilized Pt Nanoparticle Catalysts by X-ray Absorption Spectroscopy

Daniel S. Gatewood,[†,‡] Terence L. Schull,[†] Olga Baturina,[§] Jeremy J. Pietron,[†] Yannick Garsany,[†] Karen E. Swider-Lyons,[†] and David E. Ramaker*[,†,‡]

Chemistry Division, Naval Research Laboratory, Washington, District of Columbia 20375, Chemistry Department, George Washington University, Washington, District of Columbia 20052, and Nova Research, Incorporated, Alexandria, Virginia 22308

Received: October 1, 2007; In Final Form: December 19, 2007

The synthesis, preparation, and electrochemical characterization of triphenylphosphine triphosphonate (TPPTP) stabilized Pt particles have been reported previously with the observation that the TPPTP ligands increase the specific activity of Pt for the oxygen reduction reaction (ORR). In this work the ORR activity of the Pt/TPPTP electrocatalyst is probed by analyzing water activation with Pt L_3-edge X-ray absorption spectroscopy and the EXAFS and Delta XANES analysis techniques. The results are compared with that for similarly prepared Pt/C and Pt stabilized by an oxidized TPPTP ligand (Pt/ox-TPPTP). The Pt particles in the Pt/TPPTP catalyst at 0.54 V (RHE) are complexed via the P (i.e., Pt−P<tp) with about 0.3 ML of TPPTP. Approximately one-half of this converts to a Pt−O−P<tp linkage at 1.0 V; these species exist on the surface along with a dramatically reduced OH coverage. The reduction in OH coverage enhances the surface-specific (ORR) rate relative to the same-sized Pt particles on carbon. The Pt/ox-TPPTP catalysts are linked via a 3-fold coordinated Pt≡O−P<tp, which severely blocks sites and makes the electrocatalysts almost inactive to water activation and the ORR. The relative importance of site blocking, hydrophobic effects, and electronic effects are discussed with hydrophobic effects believed to dominate in the Pt/TPPTP catalyst and site blocking in the Pt/ox-TPPTP catalyst.

Introduction

One of the major obstacles to increasing the efficiency of proton-exchange membrane fuel cells (PEMFCs) is the slow kinetics of the oxygen reduction reaction (ORR, eq 1) at the cathode.

$$O_2 + 4H^+ + 4e^- \rightarrow 2H_2O \quad (1)$$

For platinum catalysts in aqueous acid electrolytes, it is generally accepted[1−3] that the rate-limiting step of the ORR involves electron transfer to chemisorbed O_2 (eq 2).

$$O_2 \rightarrow (O_2)_{ad} \xrightarrow{e^-} (O_2)^-_{ad} \quad (2)$$

However, above 0.6 V, OH is adsorbed on the surface, resulting in an incomplete byproduct of ORR (eq 1), as well as directly from water activation

$$Pt + H_2O \rightarrow OH/Pt + H^+ + e^{-+} \quad (3)$$

This adsorbed OH is believed to inhibit the ORR due to site blocking and a possible detrimental electronic effect. Thus, another important step in the ORR is OH removal from the surface (eq 4).

$$Pt\text{-}OH \xrightarrow{e^-,H^+} Pt\text{-}OH_2 \xrightarrow{H_2O} Pt^0 \quad (4)$$

The conclusions drawn from eqs 1−4 is that electron transfer to chemisorbed oxygen is facilitated by strong bonding between the surface platinum atoms and dioxygen, but removal of surface OH is easier when the Pt−O bond is weaker. This suggests that there is an optimal Pt−O bond energy for faster ORR kinetics. Indeed, Nørskov et al. calculated that the best electrocatalyst should bind oxygen about 0.2 eV more weakly than does pure platinum.[4] The challenge, then, is how to selectively change the strength of the Pt−O bond.

One of the first and most common approaches to altering catalyst activity is the use of mixed-metal nanoparticles.[5] Bimetallic nanoparticles are known to increase the ORR rate; however, for a given elemental composition, mixed-metal nanoparticles may differ widely in atom distribution and size, depending on the manner of synthesis and activation treatment, and the enhancement is found to depend significantly on this atom distribution.[2,6] More recently, intricately designed core−shell nanoparticles consisting of Pt-atom monolayers on mixed-metal cores have shown remarkable ORR activity.[7] The effect has been interpreted to be the result of a shift of the d-band orbital energy of the surface platinum atoms.[8]

It has previously been shown that organic ligands on the surface of metal nanoparticles can significantly change the catalytic activity of certain reactions, such as the selective hydrogenation of alkynes by palladium clusters modified with 2-butyl-1,10-phenanthroline ligands.[9] Removal of the butyl group from the phenanthroline, a seemingly small change, had a profound effect on the kinetics and product distribution of the reaction. However, it is not known if the origin of this effect

* To whom correspondence should be addressed. Phone: 202-994-6934. Fax 202-994-5873. E-mail: ramaker@gwu.edu.
[†] Naval Research Laboratory.
[‡] George Washington University.
[§] Nova Research, Inc.

10.1021/jp709588c CCC: $40.75
Published on Web 03/12/2008

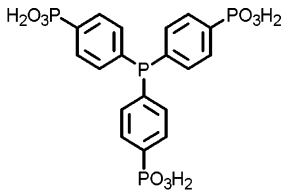

Figure 1. Water-soluble phosphine TPPTP (triphenylphosphine triphosphonate) ligand used in this work. An oxidized TPPTP (ox-TPPTP) ligand has an additional ═O group bonded to the central P atom.

is electronic in nature or due to some other physicochemical effect such as steric hindrance or hydrophobicity.

There are many examples of ligand-stabilized nanoparticles used as electrocatalysts, but in nearly all cases the ligand, typically a carboxylic acid or an amine, is exploited only to control nanoparticle formation.[10,11] These ligands are σ donors which would interact only weakly with platinum primarily through s-band orbitals if at all. However, dioxygen is known to interact with platinum through d-band orbitals, and it is of interest to know if this bonding can be perturbed by surface ligands that have significant d-orbital interaction.

Organophosphorus compounds have rich transition-metal coordination chemistry.[12] They are σ donors as well as π acceptors, which can form pπ−dπ phosphorus−metal bonds. There are a handful of examples of metal nanoparticles stabilized by phosphines,[13] although to our knowledge none of these materials have been used as electrocatalysts.

We previously reported[14,15] the synthesis, characterization, and electrochemistry of Pt nanoparticles (Pt NPs) stabilized with water-soluble phosphine TPPTP (triphenylphosphine triphosphonate, $P(4\text{-}C_6H_4PO_3H_2)_3$, see Figure 1). Aqueous solutions of these nanoparticles were used for construction of polyelectrolyte multilayers with poly(allylamine·HCl) that were grafted to glassy carbon electrodes for ORR kinetic studies using rotating disk electrode voltammetry. The Pt−TPPTP catalysts unfortunately had a lower mass activity for Pt vs the standards, making them impractical fuel cell catalysts; however, it is still useful to understand what effects change the activity of the available surface area.[15] We observed that the TPPTP ligands increased the Pt surface-specific activity of the ORR vs Pt/C standards.

Herein, we report the in-situ X-ray absorption spectroscopy (XAS) of Pt/TPPTP, Pt functionalized with oxidized TPPTP (Pt/ox-TPPTP), and compare the results with the "naked" Pt/C, i.e., without phosphine ligands. The Pt/ox-TPPTP contains a P═O bond and was predicted to have little or no direct P−Pt electronic interactions but nearly identical physical characteristics compared to the unoxidized TPPTP. Analysis of the XANES (near-edge) region of the XAS data was carried out using the $\Delta\mu$ technique[17,18] previously applied to adsorption of H, O, and OH on Pt[18] and Pt−M (M = Cr, Fe, Co, and Ni) cathodes,[2] to CO and OH adsorption on Pt−Ru anodes[19] in an electrochemical cell,[6] and even to Pt and PtRu anodes in an operating fuel cell with simulated reformate (H_2 and ppm CO)[19] or methanol.[20] The $\Delta\mu$ technique can provide not only adsorbate coverages but even binding site information (e.g., atop, bridged, 3-fold) of adsorbates such as H and O(H) on the Pt nanoparticles and will be utilized in this work to also provide information on the Pt−P linkage with the ligands as a function of potential in an electrochemical cell. The XANES is measured for an in-situ half cell containing the various catalysts at potentials from 0 to 1.1 V with utilization of the ΔXANES and extended x-ray absorption fine structure (EXAFS) analysis techniques to determine the voltage-dependent behavior of the catalysts for water activation. Potentials of 0.2 V and less are in the hydrogen adsorption region, 0.54 V is the double-layer region where the catalysts should be free of adsorbates, and potentials from 0.7 to 1.1 V are used to study oxygen or hydroxide, O(H), adsorption.

Experimental and Data Analysis

Catalyst and Electrode Preparation. Details of the catalysts synthesis and electrode preparation have been given previously[14,15,21] Briefly, glycol-stabilized Pt nanoparticles were dispersed in deaerated acetone and added to a solution of TPPTP, resulting in a homogeneous brown dispersion. This dispersion was mechanically stirred under N_2 for 1 h to allow for partial exchange of the TPPTP ligand at the platinum surface. The solvent mixture was then removed in vacuo, and deaerated water was added resulting in a transparent brown Pt colloidal dispersion. Complete exchange of the TPPTP ligand at the Pt NP surface required neutralization of the ligand with NaOH after partial exchange, precipitation with acetone, and resuspension in water followed by 2−4 days of stirring. The crude material was redispersed in a minimal amount of water and purified by gel filtration chromatography. Elemental analysis by ICP showed a Pt metal content of 48.6% and P content of 6.9%, corresponding to a Pt:TPPTP mole ratio of ∼4.5:1 for the sample used here. Assuming an empirical formula for the TPPTP ligand of $C_{18}H_{12}Na_6O_9P_4$ after neutralization of the phosphonic groups with NaOH, this gave a composition of approximately 84% $Pt_{15}(TPPTP)_{3.4}$ with the remaining 16% consisting of water of hydration[14] and perhaps some Cl ion coming from the synthesis process, the later expected to be washed out during electrode preparation. Pt/ox-TPPTP nanoparticles were produced in tandem as a minority fraction when synthesizing Pt−TPPTP but were produced in higher relative fraction when adding the ligands to the "bare" Pt nanoparticles at lower pH values. Elemental analysis yielded a Pt metal content of 12.78% and P content of 9.90%, corresponding to a Pt/ox-TPPTP mole ratio of ∼0.8:1 (i.e., 60% $Pt_{15}(TPPTP)_{15}$ and a larger component of water and Cl consistent with the greater amount of TPPTP). The Pt/C nanoparticles, prepared as described previously,[21] were supported on Vulcan carbon XC-72 (VC). Elemental analysis by ICP revealed that the composite was 7.1 ± 0.2% Pt by weight.

Inks of VC, PDAC, and Pt−TPPTP were made as follows for electrochemical evaluation. Briefly, VC was added to an aqueous solution of PDAC and sonicated for 1 h, resulting in a black suspension with no visibly aggregated carbon. Approximately 2 mg of Pt−TPPTP was added to ∼2 mL of the PDAC/VC ink, sonicated for 30 s, and then stirred for 1 h. Approximately 8−9 μL aliquots of the ink were added to glassy carbon disk electrodes polished to a mirror finish. The thin films were dried in air to yield smooth, evenly deposited composite films featuring ∼0.020 $mg_{Pt}/cm^2_{geometric}$. Inks made with Pt−TPPTP−oxide required a different formulation as the Pt/ox-TPPTP particles were only 12.8% Pt by weight (compared to 48.6% for Pt−TPPTP); the higher weight fraction of anionic ligand required a greater amount of the polycationic PDAC in the inks to achieve sufficient excess cationic charge to bind the anionic nanoparticles and ensure good suspension of the VC (vide infra). Otherwise, the procedure was similar, yielding smooth, evenly deposited composite films with ∼0.010 $mg_{Pt}/cm^2_{geometric}$. Inks of Pt/VC were made and cast as thin films on glassy carbon electrodes according to methods described elsewhere,[22] producing evenly deposited films featuring 0.020 $mg_{Pt}/cm^2_{geometric}$. Two different Pt/VC samples were utilized, one completely prepared in this work and a commercial Etek

TABLE 1: Parameters from EXAFS Fits[a]

	path	N	R (Å)	ΔE_o (eV)	σ^2 (Å^{-2})
Pt/C	0.54 V ($2 < k^1 < 12$, $1.6 < R < 3.0$)				
	Pt−Pt	6.4 ± 1	2.72 ± 0.02	9 ± 2	0.008
Pt/C	0.94 V ($2 < k^1 < 12$, $1.6 < R < 3.0$)				
	Pt−Pt	5.9 ± 2	2.72 ± 0.03	9 ± 1	0.008
	Pt−O	0.5 ± 0.5	2.12 ± 1	19 ± 4	0.005
Pt/C (ETEK)	0.54 V ($2 < k^2 < 12$, $1.6 < R < 3.0$)				
	Pt−Pt	8.5 ± 0.3	2.74 ± 0.01	8 ± 0.6	0.006
Pt/TPPTP	0.54 V ($2 < k^1 < 12$, $1.8 < R < 3.0$)				
	Pt−Pt	3.4 ± 1	2.75 ± 0.04	11 ± 5.0	0.006
	Pt−P_s	0.6 ± 0.4	2.4 ± 0.1	19 ± 10	0.005
Pt/TPPTP	0.90 V ($2 < k^1 < 12$, $1.4 < R < 3.7$)				
	PtPt	6.4 ± 2.0	2.75 ± 0.02	10 ± 2.0	0.006
	Pt−P_s	0.4 ± 0.5	2.4 ± 0.1	23 ± 9.0	0.005
	Pt−O	0.6 ± 0.3	2.2 ± 0.2	20 ± 5.0	0.003
	Pt−P_l	N_{P-O}	3.2 ± 0.2	27 ± 27	0.004

[a] Parameters for ox-TPPTP are not reported because an accurate EXAFS fit was unobtainable

sample used as a standard, so that in total four different catalysts were utilized. The one prepared in this work will be referred to as Pt/C and the latter always as the Etek sample.

The thin-film catalysts on glass carbon electrodes were characterized by cyclic voltammetry (CV) and rotating disk electrode (RDE) methods, as have been previously described,[14,15,22] vs a reversible hydrogen electrode (RHE) in 0.1 M $HClO_4$ electrolyte at room temperature. These results were used to determine the specific activity of the platinum in the catalysts for the oxygen reduction reaction at 0.9 V, both from the underpotential deposited hydrogen region in the CVs and the kinetic activity from the RDE.[15,22]

X-ray Absorption. In-situ XAS experiments were conducted at the National Synchrotron Light Source (NSLS) at Brookhaven National Laboratory in Upton, NY. XAS data, simultaneously in transmission and fluorescence mode, were taken at the Pt L_3 edge at beamline X-11B with a Si (111) double-crystal monochromator. The monochromator was detuned by 30% at 200 eV above the Pt L_3 edge (11564 eV) to minimize the presence of higher harmonics in the beam. The energy calibration was achieved by recording the XAS of a 7 μm thick Pt foil simultaneously with the sample. Reference foil transmission data were collected between the second and third detector. The fluorescence mode data were utilized in both the EXAFS and ΔXANES analysis. The NSLS storage ring operated at 2.80 GeV beam energy with ring currents between 40 and 200 mA.

The measurements were taken in an electrochemical half-cell, which was designed by the Adzic research group at Brookhaven National Lab.[23] Thick film electrodes on carbon gas diffusion layers (Etek) were made from the inks described earlier, but with higher platinum loadings (7 mg Pt cm^2). These were saturated with 0.1 M $HClO_4$ and placed in the cell. The cell was then placed in front of the beam between two detectors that collected incident (I_o) and sample (I) beam intensity as well as the fluorescence intensity. The potential was controlled by an Eco Chemie Autolab PGSTAT-30 potentiostat, and all data presented is with respect to the RHE.

XANES and EXAFS Analysis. A brief summary of the $\Delta\mu$ method is given here for clarity and to highlight slight differences from the previous method.

The absorption coefficient, μ, was obtained from the raw data using the ATHENA code developed by Ravel and Newville.[24] The preedge background is removed using the AUTOBK algorithm, described more fully elsewhere,[25] followed by normalization over the 50−200 eV (relative to the edge) range for XANES analysis. This procedure was carried out for both the sample data (fluorescence) and the simultaneous transmission reference foil data ($\ln I/I_{ref}$). The foil data were then aligned, and the resultant energy differences were transferred to the sample data, i.e., the ΔE determined for the foil at 'x' potential is added to the energy of the data at the same potential. This energy calibration corrects for shifts due to photon beam drift and other possible effects. This energy calibration is crucial for the success of the $\Delta\mu$ technique to ensure full cancellation of the atomic contribution in the XANES, which dominates the spectrum, i.e., $\Delta\mu$ is typically only about 1−5% of the total μ signal.

The difference $\Delta\mu = \mu(V) - \mu(V_{ref})$ is generally determined by subtracting the μ at an appropriate reference potential, V_{ref} (usually taken to be that potential at which the electrode is relatively free of most adsorbates) from other potentials to highlight the effect of these adsorbates. However, the choice of reference can change based on the nature of the inquiry, sample, adsorption edge, and operating conditions. In this work, the $\Delta\mu$ signals were obtained using two different types of references

$$\Delta\mu_L(V) = \mu(V, \text{Pt/TPP}) - \mu(0.54, \text{Pt/TPP}) \quad (5)$$

$$\Delta\mu_{cl}(V) = \mu(V) - \mu(0.54, \text{Pt/C}) \quad (6)$$

Here the notation subscript 'L' is used when the ligand-stabilized catalysts are used as reference and 'cl' when the Pt/C catalyst is used as the reference. As will be shown below, use of both eqs 5 and 6 is advantageous for bringing out different features of the adsorbates, eq 5 highlighting O(H) adsorption in the presence of the ligand and eq 6 highlighting the ligand adsorption itself. The $\Delta\mu$ were smoothed to remove random noise using a standard Savitzky−Golay smoothing routine with a 1.5 eV range.

The EXAFS analysis was performed using the Artemis code,[24] and several paths were included in the fits for each sample: either Pt−Pt, Pt−P<, and/or Pt−O−P< as indicated. Here the < sign indicates bonding to the tp (triphenyl) groups; however, the tp groups themselves were not included in the FEFF8 calculations since they would have a relatively small effect on the Pt−P scattering. The Debye−Waller factor was held at some fixed value as indicated in Table 1 for all fits to reduce scatter in the coordination numbers (CNs), and FEFF8 was used to calculate all of the other needed parameters including the many-body S_o^2 factor.

FEFF 8.0 Calculations. The FEFF 8.0 code was used to model the adsorbate $\Delta\mu_{theo}$ signatures. The $\Delta\mu_{theo}$ was determined by subtracting the μ of a clean "Janin"[26] type Pt_6 cluster"

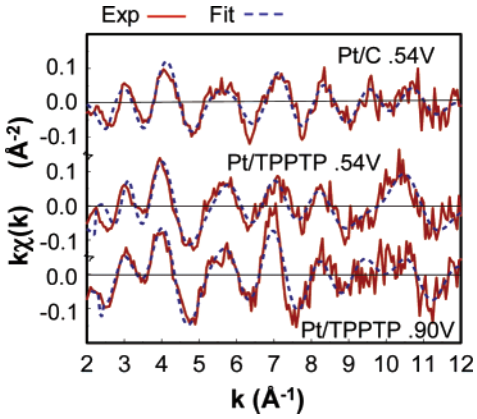

Figure 2. Comparison of the experimental EXAFS signal, $k\chi(k)$, for the Pt/C and Pt/TPPTP catalysts (at the indicated potentials) along with the fits as described in Figure 3.

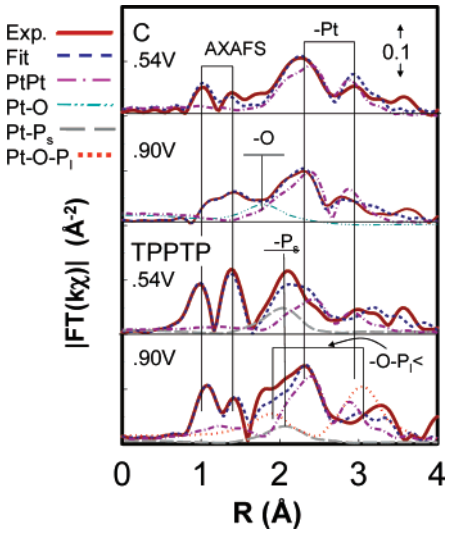

Figure 3. Comparison of $FT(k\chi(k))$ for the Pt/C and Pt/TPPTP (at 0.54 and 0.90 V) catalysts along with the fits. Also shown are the individual paths as indicated. The subscripts s and l refer to short and long Pt−P distance. The Pt−O−P_l contribution is actually the sum of the 2- and 3-step multiple scattering paths involving the Pt−O and Pt−O−P_l atoms with the fit parameters as in Table 1. Experimental uncertainty in *FT* estimated to be ±0.007.

from the μ of a cluster containing an adsorbate molecule in the atop, bridged, or *n*-fold position (as illustrated in Figure 9), e.g., $\Delta\mu_{theo}(O) = \mu(O/Pt_6) - \mu(Pt_6)$. The Janin cluster, used in much but not all of our previous work,[16−20] was chosen here because it is about the smallest cluster that contains atop, bridged, fcc, and hcp sites. The bond distances used in the clusters were the same as those in our previous FEFF 8.0 calculations.[6,19] Oxygen in the atop position was treated as OH (since the scattering from H is negligible), while oxygen in an *n*-fold position was treated as O. This is consistent with chemical intuition and density functional theory calculations,[27] which show that OH prefers to be singly coordinated and O doubly or triply.

Results

EXAFS Results. Figures 2 and 3 show EXAFS results for Pt/C and Pt/TPPTP at the indicated potentials in both *k* space and *R* space (the Fourier transform). These figures reveal the quality of the data and the fits. The relatively large noise level is clearly revealed in Figure 2 for $k > 6$ and with the signal for $k > 14$ dominated by noise. This arises in part because of the low Pt loading (16 mg Pt/g catalyst (TPPTP + PDAC + VC))

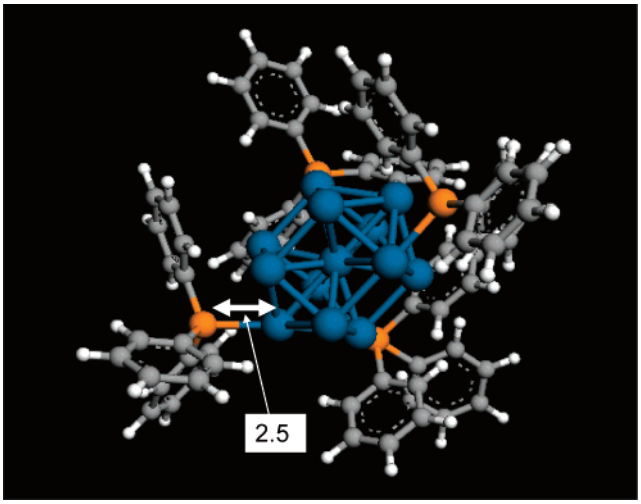

Figure 4. Illustration of a 13-atom Pt cluster and 4 TPPTP ligand groups linked through the P atom (the PO_3H_2(phosphonate) groups attached to the phenyl groups to make the ligands soluble in water are not shown). Figure constructed using the Arguslab software,[31] which performs a simple molecular mechanics (MM) calculation to reduce atom−atom repulsions.

in these samples and the relatively small photon flux of the beam. This requires large amounts of sample to be placed in the beam to achieve a Pt step height of about 0.5, and the large amount of support significantly scatters the light beam. Smoothing of the data and comparison to the EXAFS data for Pt/C Etek with larger Pt loadings nevertheless reveals comparability out to about $k \approx 14$. Thus, the high noise level is not expected to significantly alter the fit parameters, but it does lead to relatively large uncertainties in these fit parameters as shown in Table 1 (see much smaller uncertainties for the Etek sample). The relatively small Pt particles also introduce relatively large Pt−C contributions due to the carbon support around 1.4 Å in Figure 2 for the Pt/C sample. In Figures 2 and 3 and others below, a background (an option in the Artemis code) was included in the fits as shown. These background fits account for the relatively large atomic XAFS (AXAFS) peaks seen in these data. The AXAFS features for Pt/C are very similar to that found previously[16−20] and increase with potential exactly as found previously.[28] That for Pt/TPPTP in Figure 3 has the same doublet peak shape but is much larger apparently due to the Pt−TPPTP interaction. An increase in AXAFS with adsorbate coverage or support interaction has been noted previously.[28]

Table 1 shows that the Pt−Pt coordination number (CN_{Pt-Pt}) is around 6 for the catalysts prepared in this work, suggesting a particle size of 0.8−1 nm consisting of around 12−15 Pt atoms.[29] Previously these same particles were indicated to be around 1.7 nm, a result obtained from HRTEM. It is well known that EXAFS generally gives a lower estimate than either HRTEM or XRD Scherrer analysis[30] because EXAFS "sees' all particles apparently weighted toward the smaller ones, while HRTEM and XRD yields sizes weighted toward the larger particles. Thus, the average particle size may be somewhere around 1.3 nm. The CN_{Pt-Pt} of around 3.4 in the Pt/TPPTP catalysts does not necessarily suggest a smaller particle but rather reduced scattering due to the presence of the phosphine linkage to the Pt cluster. The CN_{Pt-P} of around 0.6 suggest that a 12−15-atom cluster should have around 4−5 TPPTP groups attached to it. Figure 4 illustrates such a geometry-optimized (molecular mechanics, MM[31]) cluster revealing how the triphenyl groups steer clear of each other and still allow significant

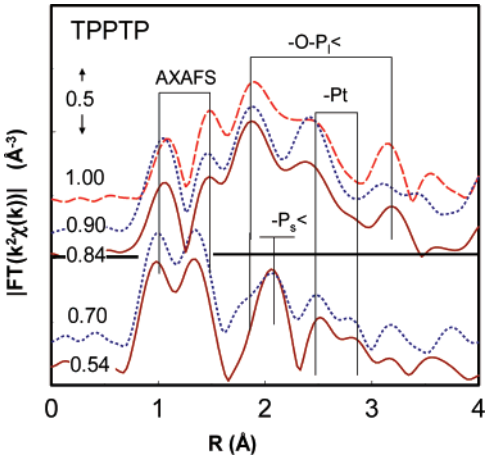

Figure 5. Variation of EXAFS spectra with potential for Pt/TPPTP with the principle peaks identified as determined from the fits in Figure 2.

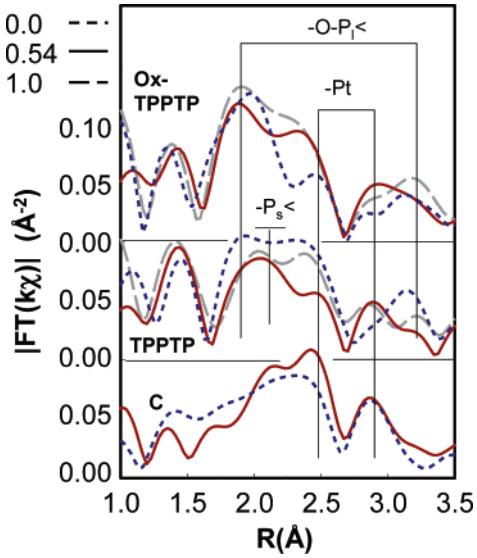

Figure 6. Comparison of the EXAFS spectra in the region between 1.0 and 3.5 Å to emphasize the Pt−P and Pt−O−P interaction for the potentials and catalysts indicated. The dominant peaks are identified as determined in Figure 2.

numbers of free Pt atoms. Atomic analysis also reveals a P/Pt ratio of about 1/4.5 consistent with the EXAFS results.[14,15]

The results in Table 1 are consistent with other EXAFS results on Pt catalysts.[2,16−20] For example, the Pt−Pt bond distance around 2.72 Å is considerably shorter than in bulk Pt (2.76 Å) or in the larger Pt particles in the C(Etek) sample as expected due to the smaller Pt coordination in these small particles. This Pt−Pt distance increases back to 2.75 Å in the Pt/TPPTP and Pt/ox-TPPTP catalysts consistent with relaxation back to the near bulk length due to complexation with the ligands. The Pt−P_s (short Pt−P distance in direct Pt−P bond) bond length of around 2.4 Å is consistent with that obtained in the molecular mechanics calculations of Figure 4. The Debye−Waller factors (σ^2) were not allowed to vary but set at fixed values typical of that seen in small Pt particles. This was to reduce the number of parameters in the fit. Finally, the ΔE_o values all appear to be larger (10−20 eV) than normal (e.g., 7−8 eV in the Etek sample), consistent with a shift of the conduction band minimum to higher binding energy in these small Pt particles as expected.

Figure 5 shows how the $FT(k^2\chi)$ for the Pt/TPPTP catalysts changes with potential. Note that as the potential increases up to 0.9 V, the Pt−O and Pt−Pt peak intensities increase while the Pt−P_s peak decreases. This suggests that the Pt−phosphine linkage breaks with an increase in potential as one might expect. However, Figure 5 shows that a peak around 3.4 Å also increases with potential, suggesting that as O adds to the cluster the TPPTP groups now link to some of the adsorbed oxygen atoms. The fit in Figure 3 already included this Pt−O−P_l scattering path for 0.9 V, and Table 1 shows that the Pt−P_l distance (the long Pt−P_l distance because of the intervening O atom) is around 3.2 Å. At potentials above 0.9 V, the Pt−Pt intensity decreases again. This is obviously due to oxidation of the Pt (i.e., Pt- and O-atom displacement and increased subsurface O atoms) as seen with all Pt particles at high potential (e.g., the Pt/C as shown in Table 1).

Figure 6 compares the $FT(k\chi)$ for Pt/C, Pt/TPPTP, and Pt/ox-TPPTP at 0, 0.54, and 1.0 V. This figure reveals the effects under reducing conditions (i.e., 0.0 V) and several important differences between the TPPTP and ox-TPPTP ligands. For Pt/TPPTP at 0.0V, the Pt−P_s peak remains, suggesting that H does not break the Pt−P linkage. The Pt−P_l peak also remains small because, of course, a Pt−H−P linkage would not occur. The Pt−Pt peak intensity is larger at 0.0 V than at 0.54 V, consistent with a change in the shape of the Pt particle from more oval-like to spherical-like with H adsorption as seen previously[16−18]

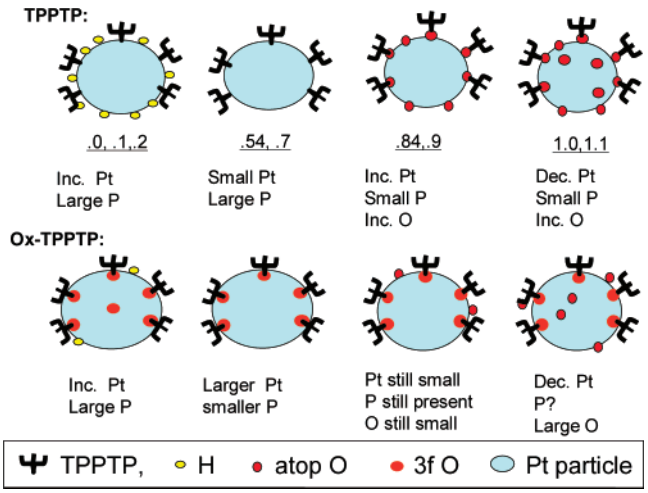

Figure 7. Summary of the changes seen in the EXAFS data with potential for the two different ligands, and the changes in the cluster ligand structure responsible for these EXAFS changes.

and perhaps some weakening (although not breaking) of the Pt−P_s bond. In contrast to the Pt/TPPTP catalysts, the Pt/ox-TPPTP catalyst does not show any breaking of the Pt−P_s bonds with potential and no sharp increase in the Pt−O−P_l peak at 1.0 V. Already at 0.54 V, a significant Pt−O peak is visible. Thus, the Pt−O−P bond remains primarily intact at all potentials in this case. This suggests that the Pt−O−P_l bonds are different in the two cases, and indeed, this will be clearly shown by examining the $\Delta\mu$ spectra below. All of these EXAFS results are summarized in Figure 7.

$\Delta\mu$ Results. Figure 8 compares the background-subtracted and normalized XANES spectra, μ, for Pt/TPPTP before subtraction. Note that the spectra are very similar beginning just 15 eV above the edge, but the differences in the region below 15 eV are well above the noise level. Figure 9 shows $\Delta\mu_{cl}$ experimental spectra (eq 6) for Pt/TPPTP and Pt/ox-TPPTP at 0.54 and 1.0 V with FEFF8 calculated $\Delta\mu_{theo}$ signatures obtained with various adsorbates on the Pt_6 Janin cluster[26] such as that illustrated in Figure 9. Since the experimental $\Delta\mu_{cl}$ spectra are shown here, the experimental signatures should reflect both the P<tp and O−P<tp adsorbates as well as O,

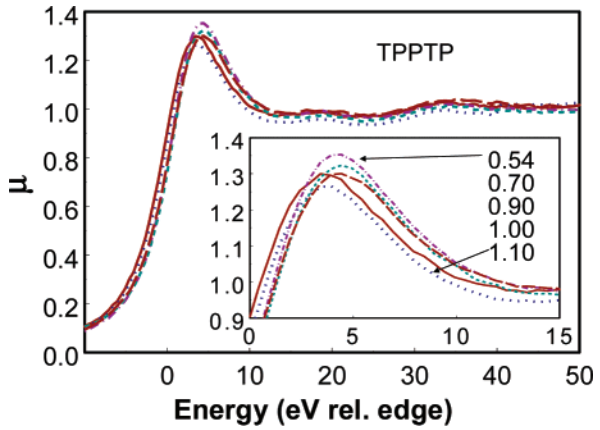

Figure 8. Comparison of background-subtracted and normalized XANES spectra, μ, for the Pt/TPPTP catalysts at the indicated potentials (V relative RHE). Both expanded (insert) and full-scale spectra are shown for comparison (lines in the full scale are identical to those in the expanded scale).

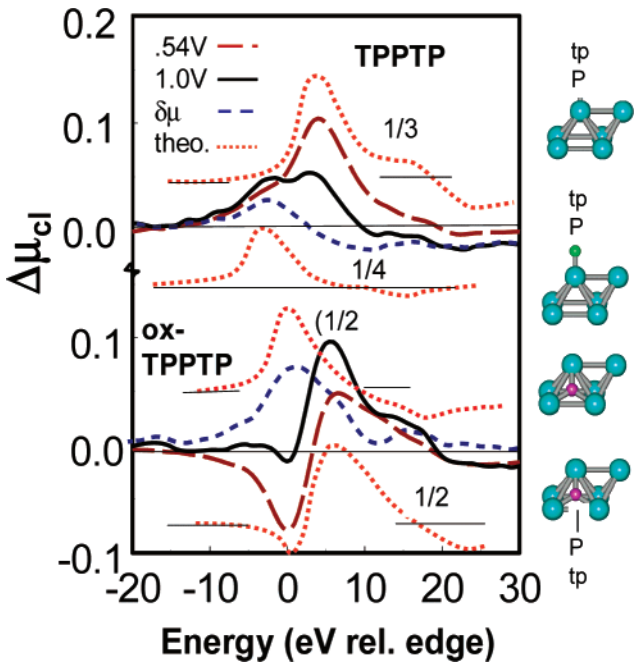

Figure 9. Comparison of experimental $\Delta\mu_{cl}$ (see eq 6) at 0.54 and 1.0 V for TPPTP and ox-TPPTP with FEFF8 calculated $\Delta\mu_{theo}$. The $\Delta\mu_{theo}$ values were calculated using the Pt_6 cluster and the adsorbates as indicated in the figure and described in the text. The clusters illustrate from top to bottom the −P<tp, −O−P<tp, ≡O, and ≡O−P<tp adsorbates on the Pt clusters. Scale factors applied to $\Delta\mu_{theo}$ are also indicated. The $\delta\mu$ difference spectra are obtained as described in the text.

where for brevity we use P<tp to represent bonding to the triphenyl groups. At 0.54 V the experimental $\Delta\mu_{cl}$ spectra are nicely reproduced by $\Delta\mu_{theo}$ for −P<tp and ≡O−P<tp adsorbates for the TPPTP and ox-TPPTP catalysts, respectively. Here '−' represents atop and '≡' 3-fold fcc coordination on the Pt. These $\Delta\mu$ results very clearly reveal yet another difference between the two catalysts and why in the latter case the ≡O−P<tp adsorbate appears to be fixed on the Pt surface at all potentials.

The relative magnitudes of the $\Delta\mu_{theo}$ and experimental $\Delta\mu_{cl}$ can be used to estimate adsorbate coverages since the $\Delta\mu_{theo}$ were calculated with a single adsorbate molecule next to the Pt absorber atom. In Figure 9 the −P<tp signature was divided by 3 and the ≡O−P<tp by 2 as indicated, suggesting a coverage

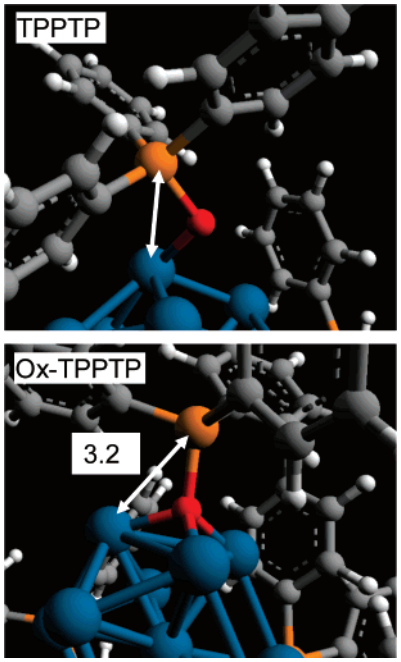

Figure 10. Molecular mechanics illustrations of the −O−P<tp and ≡O−P<tp ligand interactions obtained using Arguslab.[31] White arrows indicate Pt−P lengths which are similar in both cases.

of about 0.3 monolayers (ML) in the TPPTP case. The 0.3 ML coverage for TPPTP is entirely consistent with that indicated by the EXAFS data and the MM model in Figure 4, with about 4 TPPTP ligands adsorbed on a 13 Pt-atom cluster. The effective coverage in the 3-fold case is a bit more difficult to estimate. Each adsorbate molecule in a 3-fold site is coordinated to three Pt atoms (this would suggests a coverage, ox-TPPTP molecules/Pt atom, of only 0.5/3 = 0.16 ML), but each ligand in a 3-fold site may block three or more Pt atoms, so that one-half or more of the Pt atoms may be blocked by the ligand. Because of the bulky nature of the ox-TPPTP ligand, this is highly likely; therefore, an effective site-blocking coverage of 0.5 ML or more is expected, consistent with what will be evident below.

Next we consider the experimental $\Delta\mu_{cl}$ signatures at 1.0V. That for TPPTP clearly shows about a 50% reduction in the −P<tp coverage and then addition of another component at lower energy. Obtaining the difference $\delta\mu = \Delta\mu_{cl}(1.0V) - 0.5\,\Delta\mu_{cl}(0.54\ V)$ isolates this component and gives a signature very similar to $\Delta\mu_{theo}$ for −O−P<tp, suggesting now an atop −O−P<tp ligand coordination. The relative magnitudes between theory and experiment then suggest that about one-half of the existing −P<tp at 0.54 V (0.15 ML) is converted to −O−P<tp at 1.0 V (this is consistent with the EXAFS). In contrast, no reduction in the ≡O−P<tp component is seen for the ox-TPPTP, and addition of a ≡O component appears. However, the coverage is probably much less than 0.5 ML suggested by the relative magnitudes between $\Delta\mu_{cl}$ and $\Delta\mu_{theo}$ in this case (we will see below that it is much less).

Figure 10 illustrates a close up of the geometry-optimized O−P<tp model in the two different catalysts. Note that the Pt−P_l distance remains around 3.2 Å in both cases consistent with the EXAFS; however, the Pt−O MM-optimized distance is around 2.2 Å for the atop and <2.0 Å for the 3-fold sites reflecting the stronger Pt−O bond in the latter case.

Figure 11 examines the H coverage at low potentials for the two catalysts. Since in general the ligand existing at 0.54 V in both catalysts is not expected to leave at low potentials, Figure 11 utilizes $\Delta\mu_L$ (eq 5) to isolate the effect of the additional H

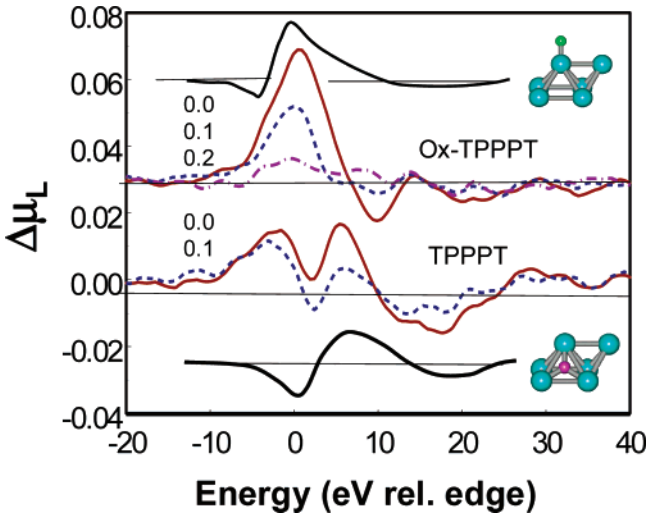

Figure 11. Comparison of $\Delta\mu_L$ (eq 5) in the H region at the indicated potentials for the two ligands. The $\Delta\mu_{theo}$ atop and 3-fold H/Pt signatures, obtained using the clusters illustrated, are shown.

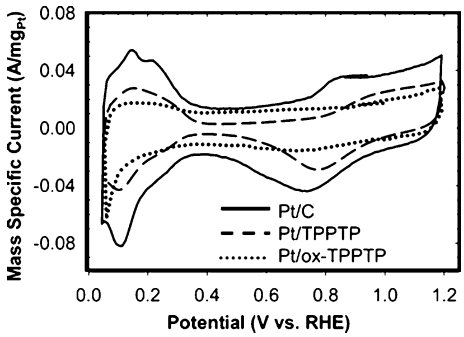

Figure 12. CV curves for the thin-film catalyst layers in 0.1 M $HClO_4$ at 25 °C. Scan rate = 50 mV/s.

adsorption. H can exist in both atop and 3-fold sites on Pt, and indeed, this is evident for the Pt/TPPTP catalysts as shown by comparison with the $\Delta\mu_{theo}$ shown in the figure. Generally, the 3-fold sites are favored on the faces and the atop H at the corners/edges of the clusters. In contrast, the Pt/ox-TPPTP catalysts show only increasing atop H as the potential is lowered to 0.0 V. Generally the corner/edges fill with H first followed by the 3-fold on the faces; indeed, the atop H existing at lower coverage often converts to 3-fold H at higher coverage. Thus, the existence of only atop H on the Pt/ox-TPPTP catalysts shows a very strong reduction in H adsorption in this case, suggesting that the 3-fold ≡O−P<tp ligands either severely block sites or exert a very strong ligand effect (this will be discussed further below).

The above results are consistent with the CV plots in Figure 12, where a dramatic reduction in H adsorption is revealed for ox-TPPTP and a normal H adsorption current appears for the TPPTP case. It appears that about one-third of the Pt sites are "blocked" even for the TPPTP case. This is consistent with about 0.3 ML of −P<tp existing on the surface, blocking these sites for H adsorption.

Finally, Figure 13 shows $\Delta\mu_L$ results to isolate the effects of O adsorption with potential for the two TPPTP catalysts and two Pt/C catalysts with different particle sizes.[18,32] Those $\Delta\mu$ spectra in Figure 13b for TPPTP are just the difference between those at potential V and that at 0.54 V in Figure 8. From previous work[18] examining OH and O adsorption on Pt, atop OH and *n*-fold O sites are occupied, and the $\Delta\mu_{theo}$ for threefold ≡O (shown in Figure 9) and atop −OH are similar except for

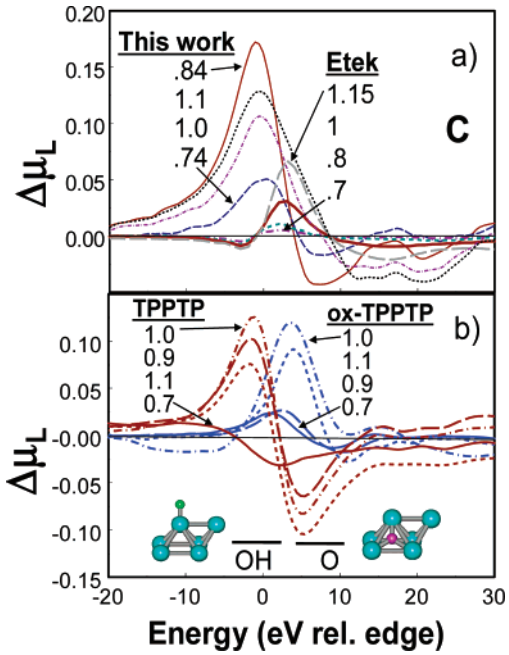

Figure 13. (a) Comparison of the experimental $\Delta\mu_L$ (eq 5) at the potentials indicated for the Pt/C studied in this work (0.8 nm), and a Pt/C Etek catalysts (2 nm)[32] to compare the effects of bigger Pt particles. (b) Same as above but now comparing the effects of the two different ligands, the Pt/TPPTP and Pt/ox-TPPTP catalysts, at the indicated potentials. The regions where the $\Delta\mu$ signatures should show maxima for OH and O on Pt are also indicated.

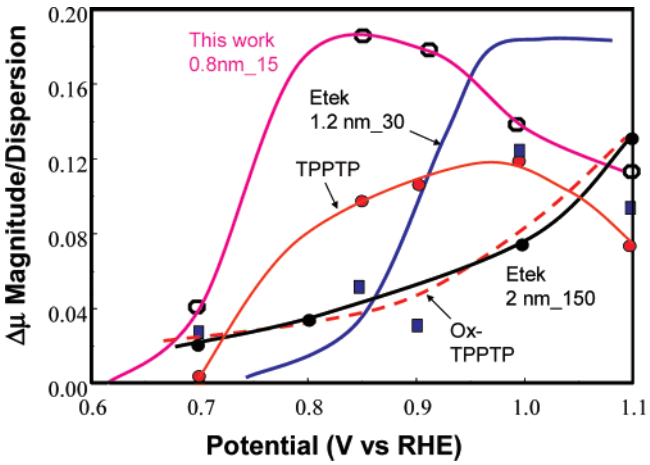

Figure 14. Plot of $\Delta\mu_L$ magnitudes corrected for the dispersion vs potential for three[4] different Pt catalysts C, Etek, TPPTP, and ox-TPPTP studied in this work and another Pt Etek catalysts (1.2 nm_30) studied previously.[18,32] The notation *xx* nm_*yy* indicates the estimated cluster diameter and number of Pt atoms for the Pt/C catalysts assuming the particle size obtained from EXAFS. The cluster sizes for the ligand-stabilized catalysts are assumed to be the same as the 0.8nm 15.

an ∼5−7 eV energy shift as indicated in Figure 13. Note that the signature for *n*-fold O is seen in the ox-TPPTP case because the ≡O−P<tp ligand is not leaving, and hence, its contribution is canceling out in the difference technique, but the OH signature for the TPPTP case has a large negative contribution between 3 and 10 eV that is inconsistent with the OH theoretical signature. This arises of course because the −P<tp ligand is converting to −O−P<tp with potential, as shown in Figure 7. Nevertheless, we shall utilize the magnitude of the experimental $\Delta\mu_L$ signatures in both cases as representative of the relative amount of O(H) adsorption in Figure 14.

Figures 13a and 14 show the dramatic effects of particle size. Atop OH is preferred at the corners and edges, and since these

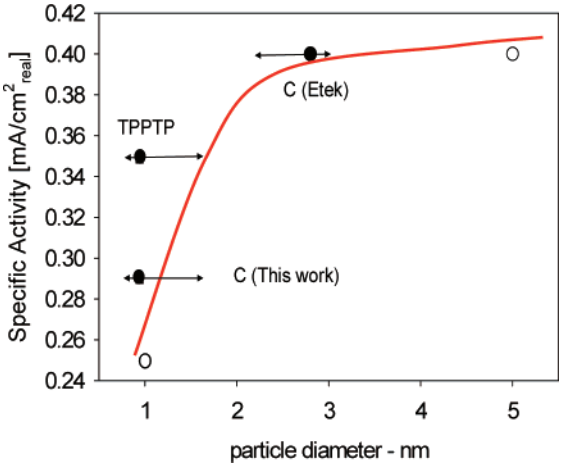

Figure 15. Surface-specific ORR activity of platinum for four catalysts studied in this work and for those reported by Mayrhofer et al.[33] (open circles). The solid line is the optimal plot through the Pt/VC catalysts and shows the sharp change with particle diameter similar to that reported previously by Kinoshita.[35] Uncertainty in particle diameters are indicated for the small particles discussed in this work with the lower limit given by the EXAFS analysis in this work and the higher limit from the HRTEM[14,15] as discussed in the text.

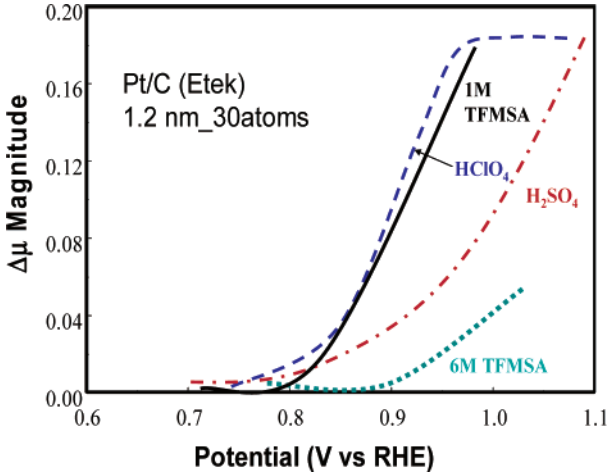

Figure 16. Previously reported[36] $\Delta\mu$ magnitudes indicating relative OH coverage as a result of water activation in the indicated electrolytes. Results are shown for 0.1 M $HClO_4$ and H_2SO_4 as well as for 1 and 6 M TFMSA. The average cluster size is indicated for all results.

sites dominate on very small particles, mostly OH exist on small particles, while on the big Pt_{etek} particles a very small amount of OH at 0.7 V is quickly overwhelmed by *n*-fold O at higher potential. Figure 13b shows a similar domination of atop OH in the TPPTP case but a surprising early transition to *n*-fold O above 0.9 V. Figure 14 shows that at least a 300 mV shift to lower potential occurs in O(H) adsorption as the particles get smaller. This shift has been noted previously by others, either by examining CV curves[33] or with a similar $\Delta\mu$ technique.[6] In Figure 14 reduction of the $\Delta\mu_L$ magnitudes at higher potential reflects the O going subsurface, since subsurface O has been shown previously[18] to have a slightly different $\Delta\mu$ spectral shape with a smaller magnitude between 0 and 5 eV.

Figures 13 and 14 also reveal the effects of the phosphine ligands. The Pt/ox-TPPTP shows a dramatic reduction in O(H) adsorption consistent with the CV curve in Figure 12. Clearly the ≡O−P<tp ligand severely blocks both H and O(H) adsorption, but a very interesting difference is seen in the binding sites for this catalysts; H appears to adsorb mostly on the corner/edge sites and O (apparently) on the face sites. This will be discussed in light of a possible electronic effect in the next section. Furthermore, the Pt/TPPTP catalyst shows a significant shift of the OH adsorption to higher potential compared with the Pt/C catalysts, consistent with the CV curve in Figure 12. Note that the $\Delta\mu_L$ magnitude compared with $\Delta\mu_{theo}$ for the Pt/C (0.8 nm) catalysts (not shown) reveals a 1 ML coverage at 0.8 V, while we concluded above that the combined −O−P<tp and −P<tp coverages were only about 0.3 ML. Thus, the difference in O coverage is even larger than the relative difference in $\Delta\mu_L$ magnitudes shown in Figure 14.

Discussion

The results above reveal significant effects of both particle size and phosphine ligands on O(H) and H adsorption. OH adsorption is known to dramatically alter the oxygen reduction ORR, as OH poisons sites where the ORR might occur.[34] Although the particle size effect on ORR has been attributed to other effects such as geometric site dependencies for the ORR,[35] it is generally accepted now that OH adsorption is the critical factor. This can be made more evident here again by examining the specific ORR activity with particle size, as shown in Figure 15. Recent results for Pt/C are shown along with those for the catalysts examined in this work.[15] Factors of 5 and even larger differences in specific reactivity have been seen between very large particles (≫5 nm) and small ones[33,35] even though the range shown in Figure 15 shows a factor of only 2.

We discuss here the role of site blocking and hydrophobic and electronic effects on O(H) adsorption due to water activation, the reaction studied in this work, as well as the ORR. To distinguish these effects more clearly, Figure 16 shows previously reported[36] $\Delta\mu$ results (reflecting relative O(H) coverage as above) on Pt/C clusters of around 1.2 nm in different electrolytes. Adsorption of O(H) in 0.1 M $HClO_4$ and 1 M TFMSA is similar because anion adsorption does not occur in either case. The upward shift in O(H) adsorption in 0.1 M H_2SO_4 of course arises because of bisulfate adsorption, but the mechanism here may be either simple site blocking or an electronic effect because of the negative bisulfate anion. Wang et al.[37] separated these two effects on the ORR and concluded that between 500 and 900 mV detrimental electronic effects from the charged bisulfate anion dominate but that OH adsorption primarily acts through simple site blocking between 700 and 950 mV. Figure 16 shows that 6 M TFMSA impedes OH adsorption from water activation even more, but it has been shown that in 6 M TFMSA anion adsorption also occurs. In spite of the anion adsorption in 6 M TFMSA, the ORR rate is generally larger in 6 M TFMSA than in 1 M TFMSA.[38] Apparently in 6 M TFMSA, anion adsorption actually helps the ORR rate, and this occurs apparently because of the concentration and/or hydrophobic effects, which keep water away from the Pt surface and reduces OH poisoning. It follows that in 6 M TFMSA reduction of OH adsorption more than compensates for the sites which may be poisoned by the TFMSA anion adsorption. Indeed, a significant motivation for this work[14,15] was that a neutral and hydrophobic ligand such as TPPTP might be ideal. It has the hydrophobic phenyl groups that may act similar to the hydrophobic F groups in TFMSA yet provides a neutral ligand, which hopefully will lower the detrimental electronic effects that are severe with bisulfate and probably also TFMSA on the ORR.

Figure 15 reveals that the TPPTP ligand does indeed improve the surface-specific ORR rate on small particles; the surface-specific ORR rate is larger in the Pt/TPPTP catalysts than for

the similarly sized Pt particles in Pt/C (0.8 nm) catalysts. This arises no doubt because, in spite of the adsorbed phosphine ligands that block sites, the OH poisoning is reduced. This leaves the question, is the reduced OH adsorption due to the hydrophobic effect or an electronic effect? One would expect H adsorption to experience an electronic effect as well if it existed. However, Figure 11 shows a remarkable similarity between the CV curves in the H region for both Pt/C and Pt/TPPTP. This suggests that indeed the neutral TPPTP ligand may not be exhibiting much of an electronic effect as expected and that indeed the hydrophobic effect is dominating.

Finally, we consider the strange difference between the H and O(H) adsorption in the Pt/ox-TPPTP catalyst. The atop H adsorption seen at low potentials may in fact be on top H adsorption, i.e., adsorption on top of those Pt sites already involved in bonding to the ligands. On top H is known[16−18] to adsorb in the presence of 3-fold 'underpotential deposited" (UPD) H, so perhaps it can adsorb in the presence of the 3-fold phosphine ligands as well, in precisely the same potential range as normal. This would suggest that the 3-fold sites are mostly blocked by the ≡O−P<tp ligands. However, the O(H) adsorption appears to behave similar to large particles, i.e., initially a small atop OH component followed early on by *n*-fold O (Figure 14), albeit at low overall coverage. This *n*-fold O adsorption may indeed be 2-fold bridged O, which is known to adsorb early on at step edges (the $\Delta\mu$ technique cannot distinguish between 2- and 3-fold bonded O). The transition from OH to O is dependent on the relative Pt−O bond strength. At normal corners and edges the Pt−O bond strength is very large,[39] so the OH prefers to stay as it is rather than moving to a bridged or fcc site. If indeed most of the Pt atoms are already bonded to an adsorbed ligand, this will weaken the Pt−OH bond, enabling early transition to bridged O. Thus, the H and O adsorption sites (although different) may indeed simply be reflecting a weakened adsorption bond due to prebonding with a ligand (i.e., a type of electronic effect) in the ox-TPPTP catalysts.

Conclusions

The conclusions from this work can be summarized as follows. (1) The TPPTP ligands partially block Pt sites but reduce water activation, most likely due to the hydrophobic effect which reduces water concentrations near the surface and therefore enhances the Pt surface-specific ORR activity. Unfortunately the mass-specific ORR activity is not enhanced,[15] apparently because the ligand site blocking effect is larger than the reduction in OH poisoning. Thus, the primary motivation for this study, to enhance the ORR rate by utilizing the TPPTP ligands, has been only partially met. (2) The ox-TPPTP ligands appear to exert a large electronic effect but dramatically block sites (apparently because they lie in 3-fold fcc sites), making these catalysts inactive for ORR. (3) The combination of EXAFS with the $\Delta\mu$ technique provides significant details on cluster size, ligand coverages, binding sites, and change in ligands from P<tp to O−P<tp, which correlate with and significantly complement the CV data. This is the first application of the ΔXANES technique to such complex ligands, and the success here reveals again its enormous applicability to study and characterize catalysts in situ.

Acknowledgment. We are grateful to the Office of Naval Research for funding through the NRL Nanoscience Institute for support of this research. Y.G. is a National Research Council Postdoctoral Fellow.

References and Notes

(1) Wang, J. X.; Markovic, N. M.; Adzic, R. R. *J. Phys. Chem. B* **2004**, *108*, 4127.

(2) Teliska, M.; Murthi, V. S.; Mukerjee, S.; Ramaker, D. E. *J. Electrochem. Soc.* **2005**, *152*, A2159.

(3) Anderson, A. B.; Albu, T. V. *J. Electrochem. Soc.* **2000**, *147*, 4229.

(4) Stamenkovic, V.; Mun, B. S.; Mayrhofer, K. J. J.; Ross, P. N.; Markovic, N. M.; Rossmeisl, J.; Greeley, J.; Nørskov, J. K. *Angew. Chem., Int. Ed.* **2006**, *45*, 2897.

(5) Chan, K.-Y.; Ding, J.; Ren, J.; Cheng, S.; Tsang, K. Y. *J. Mater. Chem.* **2004**, *14*, 505.

(6) Scott, F. J.; Mukerjee, S.; Ramaker, D. E. *J. Electrochem. Soc.* **2007**, *154*, A396.

(7) Zhang, J.; Lima, F. H. B.; Shao, M. H.; Sasaki, K.; Wang, J. X.; Hanson, J.; Adzic, R. R. *J. Phys. Chem. B* **2005**, *109*, 22701.

(8) Bligaard, T.; Nørskov, J. K. *Electrochim. Acta* **2007**, *52*, 5512.

(9) Schmid, G.; Mailhack, V.; Lantermann, F.; Peschel, S. *J. Chem. Soc., Dalton Trans.* **1996**, 589.

(10) Ye, H.; Crooks, R. M. *J. Am. Chem. Soc.* **2005**, *127*, 4930.

(11) Markarian, M. Z.; Harakeh, M. E.; Halaoui, L. I. *J. Phys. Chem. B* **2005**, *109*, 11616.

(12) Cotton, F. A.; Wilkinson, G.; Murillo, C. A.; Bochmann, M. *Advanced Inorganic Chemistry*, 6th ed.; John Wiley & Sons: New York, 1999;Chapter 10.

(13) Examples: (a) Gold: Woehrle, G. H.; Brown, L. O.; Hutchison, J. E. *J. Am. Chem. Soc*. **2005**, *127*, 21723. (b) Platinum: Yang, J.; Lee, J. Y.; Too, H.-P.; Valiyaveettil, S. *J. Phys. Chem. B* **2006**, *110*, 125. (c) Palladium: Son, S. U.; Jang, Y.; Yooon, K. Y.; Kang, E.; Hyeon, T. *Nano Lett.* **2004**, 4, 1147. Rhodium: Glöcker, J.; Klütze, S.; Meyer-Zaika, W.; Reller, A.; Gárcia- Gárcia, F. J.; Strehblow, H.-H.; Keller, P.; Rentschler, E.; Kläui, W. *Angew. Chem., Int. Ed.* **2007**, *46*, 1164.

(14) Kostelansky, C. N.; Pietron, J. J.; Chen, M.-S.; Dressick, W. J.; Swider-Lyons, K. E.; Ramaker, D. E.; Stroud, R. M.; Klug, C. A.; Zelakiewicz, B. S.; Schull, T. L. *J. Phys. Chem. B* **2006**, *110*, 21487.

(15) Pietron, J. J.; Garsany, Y.; Baturina, O.; Swider-Lyons, K. E.; Ramaker, D. E.; Schull, T. L. *Electrochem. Solid State Lett.*, submitted for publication.

(16) Koningsberger, D. C.; de Graaf, J.; Mojet, B. L.; Ramaker, D. E.; Miller, J. T. *Appl. Catal. A* **2000**, *191*, 205. Mojet, B. L.; Miller, J. T.; Ramaker, D. E.; Koningsberger, D. C. *J. Catal.* **1999**, *186*, 373. Ramaker, D. E.; Mojet, B. L.; Garriga Oostenbrink, M. T.; Miller, J. T.; Koningsberger, D. C. *Phys. Chem. Chem. Phys.*, **1999**, *1*, 2293. Koningsberger, D. C.; Oudenhuijzen, M. K.; Bitter, J. H.; Ramaker, D. E. *Top. Catal.* **2000**, *10*, 167. Mojet, B. L.; Ramaker, D. E.; Miller, J. T.; Koningsberger, D. C. *Catal. Lett.* 1**999**, *62*, 15.

(17) Ramaker, D. E.; Koningsberger, D. C. *Phys. Rev. Lett.* **2002**, *89*, 139701.

(18) Teliska, M.; O'Grady, W. E.; Ramaker, D. E. *J. Phys. Chem. B* **2004**, *108*, 2333. Teliska, M.; O'Grady, W. E.; Ramaker, D. E. *J. Phys. Chem. B* **2005**, *109*, 8076.

(19) Scott, F. J.; Roth, C.; Ramaker, D. E. *J. Phys. Chem. C* **2007**, *111*, 11403.

(20) Roth, C.; Benker, N.; Buhrmester, T.; Mazurek, M.; Loster, M.; Fuess, H.; Koningsberger, D. C.; Ramaker, D. E. *J. Am. Chem. Soc.* **2005**, *127*, 14607.

(21) Wang, Y.; Ren, J. W.; Deng, K.; Gui, L.; Tang, Y. *Chem. Mater.* **2000**, *12*, 1622.

(22) Gasteiger, H. A.; Kocha, S. S.; Sompalli, B.; Wagner, F. T. *Appl. Catal. B: Environ.* **2005**, *56*, 9.

(23) Sasaki, K.; Wang, J. X.; Balasubramanium, M.; McBreen, J.; Uribe, F.; Adzic, R. R. *Electrochim. Acta* **2004**, *49*, 3873.

(24) Ravel, B.; Newville, M. *J. Synchrotron Radiat.* **2005**, *12*, 537.

(25) Newville, M.; Livins, P.; Yacoby, Y.; Rehr, J. J.; Stern, E. A. *Phys. Rev. B.* **1993**, *47*, 14126.

(26) Janin, E.; von Schenck, H.; Gothelid, M.; Karlsson, U. O.; Svensson, M. *Phys. Rev. B.* **2000**, *61*, 13144.

(27) Oudenhuijzen, M. K.; van Bokhoeven, J. A.; Ramaker, D. E.; Koningsberger, D. C. *J. Phys. Chem. B* **2004**, *108*, 20247.

(28) Mojet, B. L.; Miller, J. T.; Ramaker, D. E.; Koningsberger, D. C. *J. Catal.* **1999**, *186*, 373. O'Grady, W. E.; Ramaker, D. E.; Qian, X. *J. Phys. Chem. B* **1997**, *101*, 5624.

(29) Ramaker, D. E.; Oudenhuijzen, M. K.; Koningsberger, D. C. *J. Phys. Chem. B* **2005**, *109*, 5608.

(30) Calvin, S.; Luo, X.; Caragianis-Broadbridge, C.; McGuinness, J. K.; Anderson, E.; Lehman, A.; Wee, K. H.; Morrison, S. A.; Kurihara, L. K. *Appl. Phys. Lett.* **2005**, *87*, 233102. Calvin, S.; Miller, M. M.; Goswami, R.; Cheng, S. F.; Mulvaney, S. P.; Whitman, L. J.; Harris, V. G. *J. Appl. Phys.* **2003**, *94*, 778. Calvin, S.; Riedel, C. J.; Carpenter, E. E.; Morrison, S. A.; Stroud, R. M.; Harris, V. G. *Phys. Scr.* **2005**, *T115*, 744.

(31) Thompson, M. A. ArgusLab 4.0; Planaria Software, LLC: Seattle, WA; http://www.arguslab.com.

(32) Arruda, T. M.; Shyam, B.; Ziegelbauer, J. M.; Ramaker, D.; Mukerjee, S. Manuscript in preparation.

(33) Mayrhofer, K. J.; Blizanac, B. B.; Arenz, M.; Stamenkovic, V. R.; Ross, P. N.; Marković, N. M. *J. Phys. Chem. B* **2005**, *109*, 14433.

(34) Markovic, N. M.; Gasteiger, H.; Ross, P. N. *J. Electrochem. Soc.* **1997**, *144*, 1591.

(35) Kinoshita, K. *J. Electrochem. Soc*. **1990**, *137*, 845.

(36) Teliska, M.; Murthi, V. S.; Mukerjee, S.; Ramaker, D. E. *J. Phys. Chem. C* **2007**, *111*, 9267.

(37) Wang, J. X.; Markovic, N. M.; Adzic, R. R. *J. Phys. Chem. B* **2004**, *108*, 4127.

(38) Murthi, V. S.; Urian, R. C.; Mukerjee, S. *J. Phys. Chem. B* **2004**, *108*, 11011.

(39) Ramaker, D. E.; Teliska, M.; Zhang, Y.; Stakheev Yu, A.; Koningsberger, D. C. *Phys. Chem. Chem. Phys.* **2003**, *5*, 4492.